Carbogen Gas–Challenge BOLD MR Imaging in a Rat Model of Diethylnitrosamine-induced Liver Fibrosis[1]

Ning Jin, MS
Jie Deng, PhD
Tamuna Chadashvili, PhD
Yue Zhang, BS
Yang Guo, MD
Zhuoli Zhang, MD
Guang-Yu Yang, MD, PhD
Reed A. Omary, MD
Andrew C. Larson, PhD

Purpose: To investigate the relationship between gas-challenge blood oxygen level–dependent (BOLD) magnetic resonance (MR) imaging measurements and hepatic disease progression in a rat model of diethylnitrosamine (DEN)-induced liver fibrosis.

Materials and Methods: The institutional animal care and use committee approved all experiments. Liver fibrosis was induced in 27 male Wistar rats by means of weekly oral gavage with 5 mL of 1.5% DEN solution per kilogram of body weight for 3–11 weeks, which produced varying degrees of liver fibrosis. Eight rats developed nonsubstantial fibrosis; eight rats, substantial fibrosis; and 15 rats, cirrhosis. Four nontreated healthy rats served as controls. Multiple-gradient-echo MR images were acquired in the rats at steady-state normoxia and hyperoxia and then during dynamic gas challenges. The change in R2* (ΔR2*) during the gas challenge and the ratio of number of activated voxels to total number of voxels in the liver were quantified. Masson trichrome staining of liver tissue was used to identify collagen tissue. Liver fibrosis was assessed by using a semiquantitative METAVIR scoring system and quantitative analysis of the percentage of liver fibrosis. Hepatic hemodynamic responses at BOLD MR imaging were compared across the fibrosis stages at independent-sample *t* test and linear regression analyses.

Results: ΔR2* was well correlated with gas-challenge interval. Mean ΔR2* decreased during liver fibrosis progression, from 19.60 sec^{-1} ± 4.47 (standard deviation) in animals without substantial fibrosis to 14.02 sec^{-1} ± 2.88 and 6.26 sec^{-1} ± 7.40 in animals with substantial fibrosis and cirrhosis, respectively (P = .006 for rats without vs rats with substantial fibrosis, P = .001 for rats with substantial fibrosis vs rats with cirrhosis, $P < .001$ for rats without substantial fibrosis vs rats with cirrhosis). Mean ΔR2* ($r = -0.773$) and liver activation ($r = -0.691$) were inversely correlated with liver fibrosis ($P < .001$).

Conclusion: Carbogen gas-challenge BOLD MR imaging can depict hepatic hemodynamic alterations during the progression of fibrosis and has the potential to serve as a noninvasive, nonenhanced imaging method for liver fibrosis diagnosis and staging.

[1] From the Departments of Radiology (N.J., J.D., T.C., Y.Z., Y.G., Z.Z., R.A.O., A.C.L.), Biomedical Engineering (N.J., J.D., R.A.O., A.C.L.), and Pathology (G.Y.Y.), and Robert H. Lurie Comprehensive Cancer (R.A.O., A.C.L.), Northwestern University, 737 N Michigan Ave, Suite 1600, Chicago, IL 60611; Department of Medical Imaging, Children's Memorial Hospital, Chicago, Ill (J.D.); and Department of Bioengineering, University of Illinois at Chicago, Chicago, Ill (Y.Z.). Received March 6, 2009; revision requested April 21; revision received June 12; accepted July 1; final version accepted July 15. **Address correspondence to** A.C.L. (e-mail: *a-larson@northwestern.edu*).

Liver fibrosis involves the excessive accumulation of extracellular matrix proteins as part of the wound-healing response to chronic liver injury (1). The main causes of liver fibrosis are chronic viral hepatitis type B, chronic viral hepatitis type C, and alcohol abuse (2). Advanced liver fibrosis can lead to cirrhosis, liver failure, portal hypertension, and liver cancer, and it often requires liver transplantation as a life-saving procedure.

Liver biopsy is considered the reference standard for the diagnosis and staging of liver fibrosis. However, it is invasive, with associated pain and major complications reportedly occurring in 40.0% and 0.5% of patients, respectively (3). Sampling errors can occur owing to the heterogeneous distribution of fibrosis in the liver and the relatively small biopsy samples (4,5). Intra- and interobserver variations in histologic examinations can also lead to diagnosis error (6,7). Liver fibrosis may be reversible when the cause is identified and treated (8–10). An alternative noninvasive diagnosis and staging method would be particularly useful for serial evaluation of the effectiveness of liver fibrosis therapies. Magnetic resonance (MR) elastography (11), diffusion-weighted MR imaging (12), ultrasonographic perfusion measurements (13), transient sonoelastography (14), and dynamic contrast material–enhanced MR imaging and computed tomography (15) have been proposed as noninvasive methods of diagnosing and staging liver fibrosis.

Quantitative dynamic contrast-enhanced imaging (ie, contrast-enhanced imaging) approaches involve pharmacokinetic analysis of the passage of exogenous contrast material tracers (16). These methods offer the potential to detect and characterize the hepatic perfusion changes that accompany the progression of liver fibrosis (15). Approximately three-quarters of the blood in the normal liver is supplied from the portal vein, and only about one-quarter of the blood is supplied from the hepatic artery (17). During the evolution of hepatic fibrosis, the progressive disruption of the normal liver structure leads to both regional and global perfusion changes. Portal venous flow typically decreases and bypasses the liver parenchyma via portosystemic venous shunts, while hepatic arterial flow may increase to counteract the effect of the reduced portal venous flow. This counteractive increase in hepatic arterial flow is commonly referred to as the hepatic arterial buffer response (18,19). Quantitative contrast-enhanced imaging methods can be used to resolve each component of the dual blood supply in the liver (20). Initial preclinical and clinical feasibility studies have revealed the potential to use these differential blood flow measurements to characterize disease progression (21–23).

Blood oxygen level–dependent (BOLD) MR imaging is an alternative imaging technique that involves the use of deoxyhemoglobin as an endogenous contrast mechanism to reflect alterations in blood oxygenation, blood flow, and blood volume. Although BOLD MR imaging methods are widely used for functional activation studies of the brain (24,25), they are increasingly being used for functional imaging of tumors (26), cardiac (27) and skeletal (28) muscle, renal tissue (29), and the liver (30). BOLD MR examinations of rat liver tissue have revealed substantial increases in signal intensity at T2*-weighted imaging during hyperoxia induced by carbogen gas (95% O_2, 5% CO_2) inhalation (30), and more recent studies involving the use of a 4.7-T spectrometer in fibrotic mouse liver tissue have revealed a reduced response at gas-challenge T2*-weighted BOLD imaging compared with this response in healthy control animals (31). Gas-challenge BOLD MR imaging has the potential to serve as a noninvasive, nonenhanced method of characterizing hemodynamic processes of the liver. The purpose of our study was to investigate the relationship between gas-challenge BOLD MR imaging measurements and hepatic disease progression in a rat model of diethylnitrosamine (DEN)-induced liver fibrosis.

Advance in Knowledge

- Carbogen gas-challenge blood oxygen level–dependent (BOLD) MR imaging can depict hepatic hemodynamic changes during the progression of liver fibrosis.

Implication for Patient Care

- Carbogen gas-challenge BOLD MR imaging is a potential noninvasive, nonenhanced imaging method for diagnosis and staging in patients with liver fibrosis.

Materials and Methods

Animal Model

All experiments were approved by the institutional animal care and use committee of Northwestern University and were performed in accordance with institutional guidelines. Thirty-one adult male Wistar rats (Harlan, Indianapolis, Ind) that initially weighed 300–350 g were used for the experiments. The rats were randomly divided into control and treatment groups. Four nontreated healthy rats were used as control animals. Two authors (N.J., 2 years experience; Y.G., 1 year of experience) induced liver fibrosis in 27 rats by means of weekly oral gavage by using an 18-gauge gavage needle to inject 5 mL of 1.5% DEN solution (DEN ISOPAC; Sigma Chemical, St Louis, Mo) per kilogram of body weight.

Published online
10.1148/radiol.09090410

Radiology 2010; 254:129–137

Abbreviations:
BOLD = blood oxygen level dependent
DEN = diethylnitrosamine

Author contributions:
Guarantors of integrity of entire study, Z.Z., A.C.L.; study concepts/study design or data acquisition or data analysis/interpretation, all authors; manuscript drafting or manuscript revision for important intellectual content, all authors; manuscript final version approval, all authors; literature research, N.J., J.D., T.C., Y.Z., Y.G., Z.Z., A.C.L.; experimental studies, all authors; statistical analysis, N.J., J.D., Y.Z., Y.G., Z.Z.; and manuscript editing, N.J., J.D., Y.Z., Y.G., Z.Z., G.Y.Y., A.C.L.

Authors stated no financial relationship to disclose.

MR Measurements

All MR imaging examinations were performed by using a 3.0-T clinical MR unit (Magnetom Trio; Siemens Medical Solutions, Erlangen, Germany) with a custom-built rodent receiver coil that had an inner diameter of 7 cm (Chenguang Medical Technologies, Shanghai, China). Before being imaged, the rats were anesthetized with an upper-limb injection of ketamine (Ketaset, 75–100 mg per kilogram of body weight; Fort Dodge Animal Health, Fort Dodge, Iowa) and xylazine (Isothesia, 2–6 mg/kg; Abbott Laboratories, North Chicago, Ill). The abdomen of each rat was fixed with adhesive tape to restrict respiratory movement.

Coronal and transverse T2-weighted turbo spin-echo MR images (4500/61 [repetition time msec/echo time msec], 140° flip angle, three acquired signals) of the entire abdomen were acquired for localization. Three adjacent transverse sections through the central portion of the liver were chosen for the BOLD MR examinations. The response at BOLD MR imaging was evaluated by using quantitative R2* measurements, which were obtained by using a multiple-gradient-echo sequence (150-msec repetition time, echo train length of nine, 4.6-msec intersection spacing, 30° flip angle, 3-mm section thickness, 150-mm field of view, 192 × 76 matrix, 0.8-mm in-plane resolution, readout bandwidth of 360 Hz/pixel, 25 acquired signals).

Experimental Design

MR imaging was performed in the four healthy rats at week 0 and in four rats each 3 and 4 weeks after DEN administration; in five rats each 5 weeks after DEN administration; in two rats each 6, 7, 9, and 10 weeks after DEN administration; and in three rats each 8 and 11 weeks after DEN administration. The animals were administered room air (78% N_2, 20% O_2) and carbogen gas (95% O_2, 5% CO_2) separately through a nose cone at a rate of 15 mL/sec. After anesthesia was induced, the animals were exposed first to room air for 10 minutes to achieve steady-state normoxia. After the acquisition of steady-state room air multiple-gradient-echo MR images (4-minute acquisition time, 25 signals acquired), the rats were administered carbogen gas for a 10-minute transition period to achieve steady-state hyperoxia. After the acquisition of steady-state carbogen multiple-gradient-echo MR images, a dynamic time series of multiple-gradient-echo images were obtained for 60 minutes during gas challenges that lasted 10 minutes each: 10 minutes of carbogen inhalation then 10 minutes of room air inhalation, with two repeats of this regimen. For each gas challenge, a time series of 15 sets of multiple-gradient-echo images were obtained. Four signals were acquired for each acquisition to result in a temporal resolution of roughly 45 seconds for each quantitative R2* measurement.

Figure 1

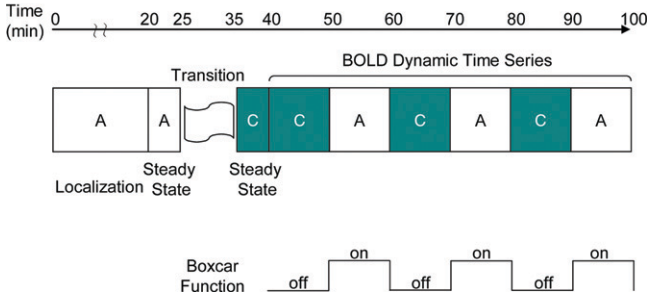

Figure 1: Experimental gas-challenge BOLD MR imaging protocol involving inhalation of room air *(A)* or carbogen *(C)*. Boxcar function, with cyclical alternations of on and off periods, was later correlated with dynamic R2* time series to produce gas-challenge liver activation maps.

Image Analysis

Image postprocessing was performed offline by one author (N.J., 2 years experience) by using Matlab software (The Math Works, Natick, Mass). Before being processed, all of the images were visually inspected to ensure that none of them were corrupted with respiratory motion–induced artifacts. R2* maps corresponding to each stage of gas inhalation and each image acquisition performed during the dynamic time series were calculated by using the nonlinear Levenberg-Marquardt algorithm to fit the monoexponential multiple-gradient-echo signal decay component: $S_{TEi} = S_0 \cdot \exp(-R2^* \cdot TEi)$, where S_{TEi} is the MR signal intensity at echo time TEi, S_0 is the MR signal intensity at echo time 0, and TEi is the echo time. Gas-challenge maps of the change in R2* (ΔR2*) were calculated by using the formula $R2^*_{air} - R2^*_{carb}$, where $R2^*_{air}$ is the R2* measurement acquired at steady-state room air multiple-gradient-echo MR imaging and $R2^*_{carb}$ is the R2* measurement acquired at steady-state carbogen multiple-gradient-echo MR imaging. On the images obtained in each animal, a region of interest that encompassed all of the liver parenchyma on each section while excluding blood vessels and gall bladder tissue was drawn. For each animal, the mean ΔR2* between the steady-state room air and carbogen breathing conditions was measured. Next, the dynamic time series of R2* values for each liver voxel was correlated by using a boxcar function that consisted of three alternating off (10-minute duration, 15 data points) and on (10-minute duration, 15 data points) time periods (Fig 1). A correlation coefficient was calculated for each voxel, and those voxels with a correlation coefficient higher than 0.4 were considered to be activated and responsive to the gas challenge. Liver activation was quantified by calculating the ratio of the number of activated voxels to the total number of voxels in the liver.

Histologic Evaluation

After the MR examinations, each rat was euthanized by means of intravenous injection of a 150 mg/kg dose of pentobarbital sodium and phenytoin sodium

Figure 2

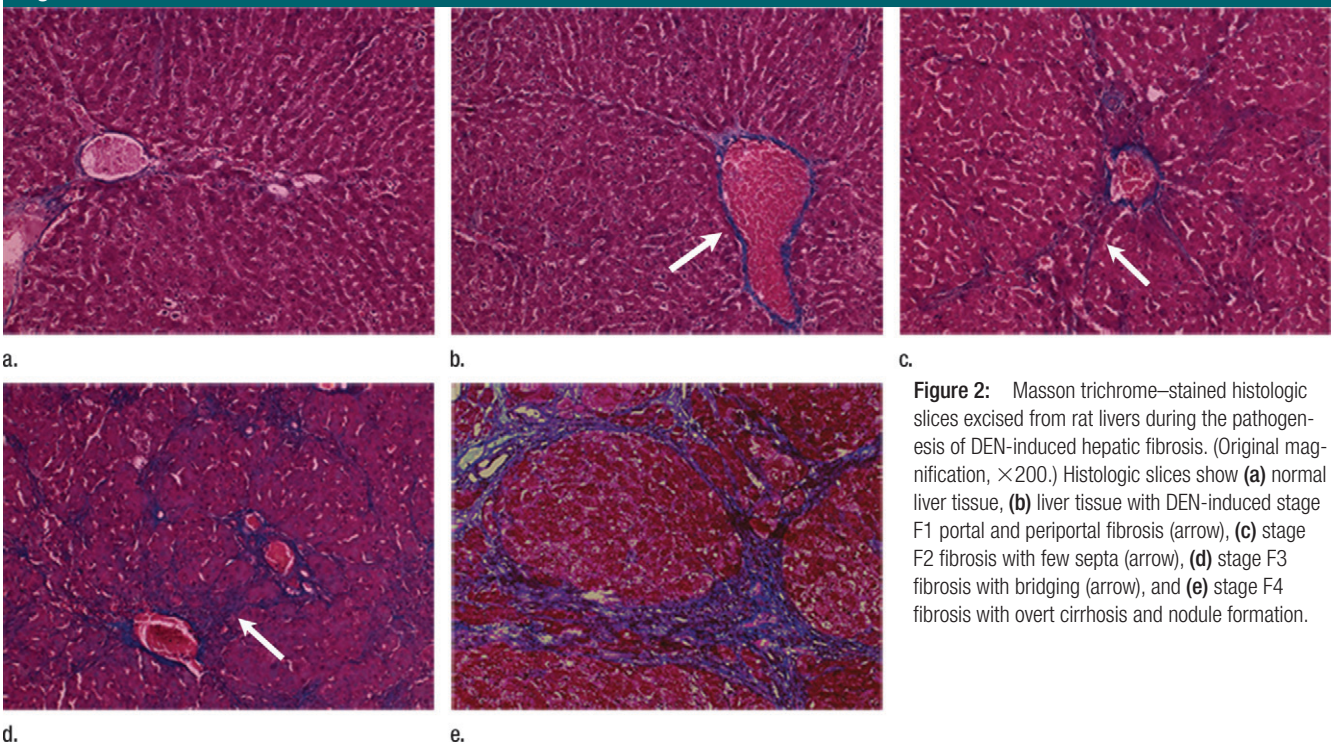

Figure 2: Masson trichrome–stained histologic slices excised from rat livers during the pathogenesis of DEN-induced hepatic fibrosis. (Original magnification, ×200.) Histologic slices show **(a)** normal liver tissue, **(b)** liver tissue with DEN-induced stage F1 portal and periportal fibrosis (arrow), **(c)** stage F2 fibrosis with few septa (arrow), **(d)** stage F3 fibrosis with bridging (arrow), and **(e)** stage F4 fibrosis with overt cirrhosis and nodule formation.

solution and bilateral thoracotomy. Three histologic slices excised from the left lateral, right lateral, and medium lateral liver lobes of each rat were fixed in 10% buffered formaldehyde solution and embedded in paraffin for histologic evaluation. Masson trichrome staining was used to identify collagen tissue. An attending surgical pathologist who specializes in gastrointestinal oncology (G.Y.Y., >10 years experience) first assessed the stage of liver fibrosis semiquantitatively according to the METAVIR scoring system: Stage F0 indicates no fibrosis; stage F1, portal fibrosis without septa; stage F2, portal fibrosis with few septa; stage F3, numerous septa without cirrhosis; and F4, cirrhosis. The Masson trichrome–stained slides were then digitized with optical magnification (×200) by using a multichannel automated imaging system (TissueGnostics, Vienna, Austria). Next, an author (N.J.) performed quantitative analysis of liver fibrosis on an average of 30 fields per section. On the stained slides, collagen fibers were stained aniline blue, while hepatocytes were stained red. The fibrotic region was identified by extracting the area of blue components with use of offline ImageJ postprocessing software (National Institutes of Health, *http://rsb.info.nih.gov/ij/*). Fibrotic deposition was expressed as the ratio of stained collagen tissue area to total area measured in the analyzed field.

Statistical Analyses

The animals were grouped into three categories (11): rats without substantial fibrosis (stages F0 and F1), rats with substantial fibrosis (stages F2 and F3), and rats with cirrhosis (stage F4). Gas-challenge $\Delta R2^*$ values were compared between the three groups at analysis of variance and then at two-by-two comparisons performed with independent-sample *t* testing.

The relationships between percentage of liver fibrosis, percentage of liver regions responsive to the gas challenge, and gas-challenge $\Delta R2^*$ were assessed by calculating Spearman correlation coefficients. Statistical analysis results were considered to be significant at $P < .05$. All statistical analyses were performed by using SPSS software (SPSS, Chicago, Ill).

Results

Five rats were found to be at stage F0 of liver fibrosis; three rats, to be at stage F1; two rats, to be at stage F2; six rats, to be at stage F3; and 15 rats, to be at stage F4 (Fig 2**)**. Carbogen inhalation induced decreases in hepatic $R2^*$ in both the healthy rats and the rats with fibrosis. The measured $\Delta R2^*$ between the room air and carbogen breathing exercises was much greater in the healthy rats than in the rats with fibrosis (Fig 3). Mean $\Delta R2^*$ values were 19.60 sec^{-1} ± 4.47 (standard deviation) for the rats without substantial fibrosis (stages F0 and F1), 14.02 sec^{-1} ± 2.88 for the rats with substantial fibrosis (stages F2 and F3), and 6.26 sec^{-1} ± 7.40 for the rats with cirrhosis (stage F4) (Table). There were significant differences in mean $\Delta R2^*$ between the animals with stages F0 and F1 fibrosis and those with stages F2 and F3 disease ($P = .006$), between the animals

Figure 3

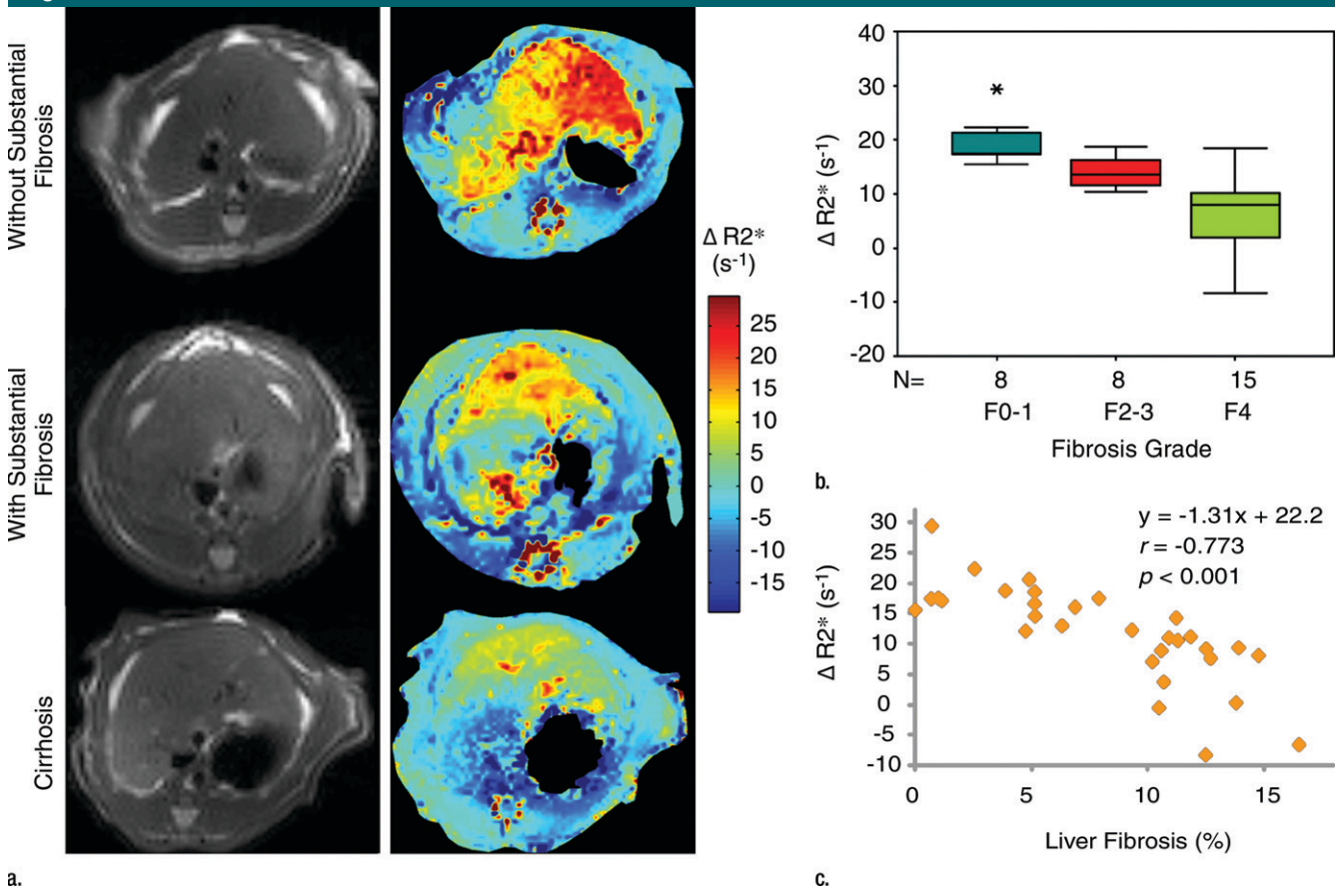

Figure 3: Decreasing gas-challenge ΔR2* with increasing fibrosis stage. **(a)** Transverse turbo spin-echo anatomic MR images (left) and corresponding gas-challenge ΔR2* maps (right) show liver without substantial fibrosis (in control rat), liver with substantial (stage F2) fibrosis, and liver with cirrhosis (stage F4). **(b)** Box plot shows mean hepatic ΔR2* values for rats in stage F0–F1, stage F2–F3, and stage F4 fibrosis groups. Bottom boundary of each box (closest to zero) indicates 25th percentile, horizontal line in each box indicates median value, and top boundary of each box (farthest from zero) indicates 75th percentile. Error bars indicate 10th and 90th percentiles. Outlier (*) is also shown. **(c)** Graph shows a significant inverse correlation between percentage of liver fibrosis *(x)* and mean gas-challenge ΔR2* *(y)* ($r = -0.773$, $P < .001$).

ΔR2* Values at Different Fibrosis Stages

Fibrosis Stage Group	No. of Rats	ΔR2* (sec^{-1})*
F0–F1	8	19.60 ± 4.47†
F2–F3	8	14.02 ± 2.88‡
F4	15	6.26 ± 7.40†‡

* Data are means ± standard deviations.

† $P < .05$ for comparison with rats in stage F2–F3 group.

‡ $P < .05$ for comparison with rats in stage F0–F1 group.

with stages F2 and F3 fibrosis and those with stage F4 disease ($P = .001$), and between the animals with stages F0 and F1 fibrosis and those with stage F4 disease ($P < .001$). We observed a significant inverse correlation between mean ΔR2* and percentage of liver fibrosis ($r = -0.773$, $P < .001$).

Two sets of dynamic time series images were excluded from our analysis owing to poor image quality caused by respiratory motion artifacts. Dynamic measurements revealed reproducible increases in R2* during room air breathing and R2* decreases during carbogen breathing in both the control rats and the rats with fibrosis (Fig 4). These processes were well correlated with the gas-challenge intervals in each animal. Most parts of the liver were activated during the gas challenge in the control animals, while liver activation decreased dramatically during fibrosis progression in the animals with fibrosis. There was a significant inverse correlation between liver activation and percentage of liver fibrosis ($r = -0.691$, $P < .001$) (Fig 5). We also observed a significant positive correlation between mean ΔR2* and liver activation ($r = 0.854$, $P < .001$).

Discussion

Liver fibrosis, the consequence of chronic liver injury from a variety of origins, is an important cause of liver dysfunction and a life-threatening disease that affects millions of individuals worldwide. As demonstrated within the

Figure 4

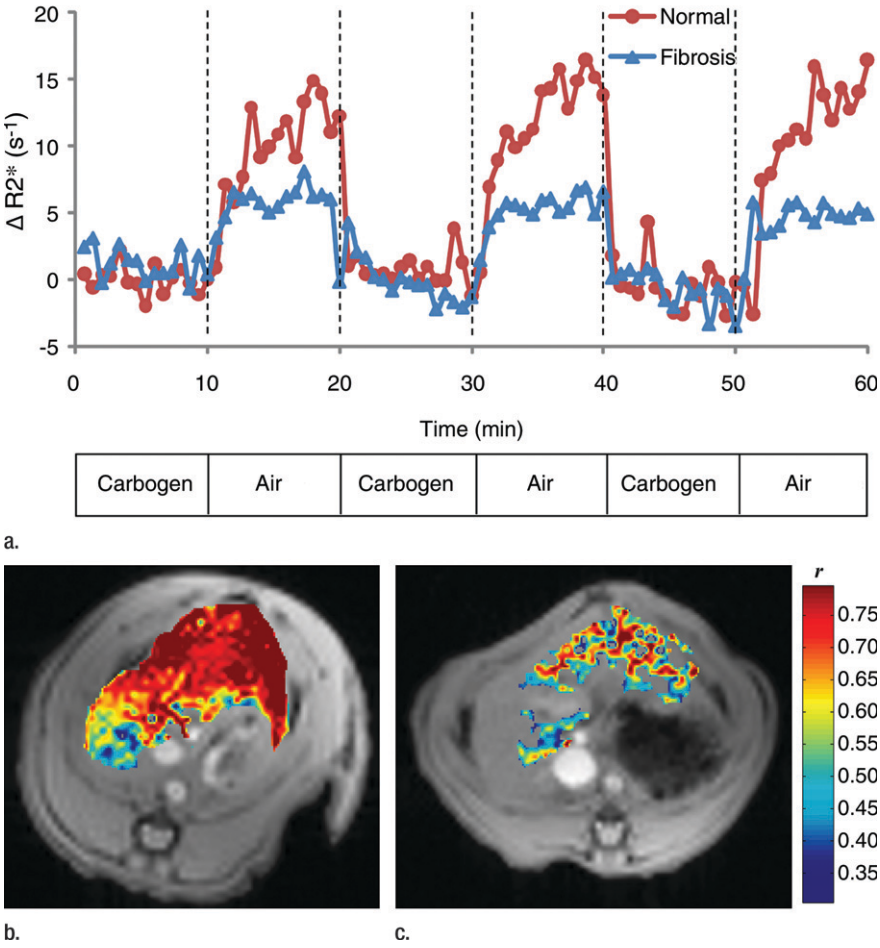

Figure 4: **(a)** Graph shows dynamic hepatic ΔR2* values in response to repeated room air and carbogen gas challenges in control rat and rat with DEN-induced fibrosis. **(b, c)** Transverse liver activation maps show hepatic regions that demonstrated a strong correlation between cyclical gas-challenge protocol and dynamic ΔR2*: A much larger portion of the liver is activated in the healthy (control) rat (**b**) than in the rat with substantial (stage F4) fibrosis progression (**c**).

past 10 years, even advanced fibrosis can be reversible with proper detection and treatment (8–10). By using noninvasive diagnosis and staging methods, one could avoid the complications and sampling errors common to biopsy procedures while facilitating close longitudinal follow-up of treatment response. MR elastography and dynamic contrast-enhanced MR imaging methods have been proposed for noninvasive staging of liver fibrosis. However, elastography requires additional transducer hardware that is not yet widely available, and quantitative dynamic contrast-enhanced MR imaging requires intravenous injection of potentially nephrotoxic contrast agents. Similar to BOLD MR methods, dynamic contrast-enhanced MR imaging methods commonly require the calculation of quantitative relaxation properties for estimation of contrast material concentration levels; however, they typically also require an additional postprocessing step that involves fitting the tissue and plasma concentration time curves to higher-order pharmacokinetic models (32). For accurate, reproducible results, the latter fitting procedures generally require high-fidelity imaging data that are relatively devoid of motion artifacts. The principal aim of our study was to investigate the use of carbogen gas-challenge BOLD MR imaging as an alternative noninvasive, nonenhanced imaging method of detecting liver perfusion alterations during the progression of hepatic fibrosis. In a rat model of DEN-induced liver fibrosis, we observed a significant inverse correlation between gas-challenge BOLD MR measurements and hepatic disease progression.

With the progression of hepatic fibrosis, we observed a significant decrease in both the gas-challenge ΔR2* and the overall area of liver activation. Both of these findings suggest a reduced hemodynamic response to the gas challenge with disease progression. This altered response may result from *(a)* a total derangement of the normal liver architecture during fibrosis development due to the presence of regenerative nodules and fibrous bands or septa between them, with resulting distortion, compression, and even obliteration of the hepatic vasculature (33); or *(b)* substantially decreased functional hepatic flow (the amount of blood circulating in the liver) due to the increased resistance of portal venous blood flow and the formation of intrahepatic portosystemic functional shunts (34).

The DEN-induced hepatic fibrosis model used in this study revealed cellular alterations and histologic patterns similar to those in human liver fibrosis (35). However, the speed of fibrosis progression varied in different animals; hence, a variable number of rats had each stage of fibrosis. DEN causes acute liver injury (inflammation and necrosis) and liver fibrosis. There was a 1-week interval between the final DEN administrations (performed weekly) and the MR examinations. We did not evaluate changes in hepatic BOLD response between the acute and chronic stages of liver injury. Future studies to examine the relationship between these functional measurements at the acute and chronic stages are warranted, particularly given the clinical relevance of such factors. Owing to the rapid progression of fibrosis in this model, a larger number of animals ended up developing later-stage (F4) fibrosis. Because of the relatively

Figure 5

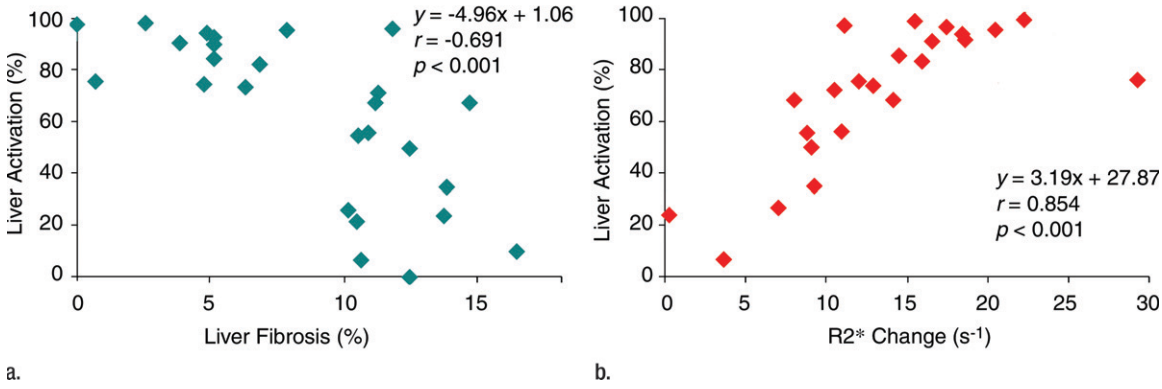

Figure 5: Regression plots show **(a)** inverse correlation between percentage of liver fibrosis *(x)* and percentage of liver activated at carbogen gas challenge *(y)* ($r = -0.691$, $P < .001$) and **(b)** strong correlation between mean observed gas-challenge $\Delta R2^*$ *(x)* and percentage of responsive liver *(y)* ($r = 0.854$, $P < .001$).

small sample, we could not compare the BOLD responses between the five METAVIR stages. Nonetheless, even with the sample size used in this initial feasibility study, we observed significant differences in gas-challenge BOLD responses between the animals in each of the three clinically relevant fibrosis groups (no substantial fibrosis [stages F0 and F1], substantial fibrosis [stages F2 and F3], and cirrhosis [stage F4]).

In previous BOLD MR studies involving the examination of mouse liver tissue, 4.7-T research MR units were used (30,31). Our current study results provide strong evidence of the immediate feasibility of clinical translation because we used a 3.0-T clinical MR unit and multiple-gradient-echo sequences that are readily available on most clinical MR systems. Furthermore, we performed quantitative $R2^*$ measurements rather than $T2^*$-weighted imaging signal intensity measurements to evaluate the gas-challenge BOLD responses. The signal intensity on gradient-echo MR images can be very sensitive to signal intensity enhancement owing to increases in blood flow, which are known as the inflow effect. This effect can lead to difficulties in distinguishing the differential contribution of blood inflow and blood oxygenation to BOLD MR imaging signal intensity changes (36). Carbogen was used to induce hyperoxia; it is safe for humans and has been applied clinically during radiation therapy to raise the oxygen tension and increase the radiosensitivity of the anoxic region (37). Compared with using pure oxygen, incorporating 5% CO_2 is believed to counteract any oxygen-induced vasoconstriction; however, further study is needed to compare the BOLD responses during oxygen gas challenges with those during carbogen gas challenges. Given the promising results of our preclinical study and the noninvasiveness of the described gas-challenge BOLD MR imaging method, translational studies involving patients with fibrosis are clearly warranted.

There were several limitations to our current study. First, we measured the mean $\Delta R2^*$ for the entire liver rather than for specific liver regions on each image section because it was difficult to coregister the MR images with the histologic specimens and because we assumed a priori that DEN-induced fibrosis would progress homogeneously in each animal's liver. However, variations in $\Delta R2^*$ and liver activation were observed and probably resulted from the differing blood supply in the different liver regions and/or the different levels of fibrosis. Future studies to further investigate these intrahepatic differences in BOLD response in specific regions or lobes in the liver should be performed. Furthermore, we did not serially follow up each animal during DEN administration and fibrosis progression; rather, we performed MR imaging in each animal at a single time point. We chose the latter approach because of the logistic complexities involved in serially following up the animals during these processes and our desire for reference-standard histologic confirmation of the fibrosis stages, which required that we sacrifice each animal to harvest their livers. In future BOLD MR studies, fibrosis progression could be followed in each animal. Finally, we determined liver activation by using a boxcar function to correlate the dynamic time series of $\Delta R2^*$ values for each liver voxel and using a correlation coefficient of 0.4 as the threshold of activation. This threshold value was chosen on the basis of previous BOLD brain activation study findings (38). While a range of threshold values seemed to yield similar results in our gas-challenge hepatic BOLD MR examinations, future studies are warranted to optimize this threshold.

The total imaging time was roughly 2 hours for each animal because we measured BOLD response during both steady-state and dynamic gas challenges. However, there was a close correlation between mean $\Delta R2^*$ and overall liver activation, suggesting that dynamic measurements may not be required. The dynamic BOLD MR measurements were useful during these preclinical examinations to demonstrate the temporal responses, but these measurements required the bulk of the overall

imaging time. While the described findings would need to be reproduced in studies involving patients, it might be possible to eliminate the dynamic measurements to reduce the overall imaging time and facilitate clinical translation. In addition, respiratory motion during abdominal imaging can be problematic, particularly in clinical settings, with motion artifacts introducing substantial errors on reconstructed $R2^*$ maps. For application of the described gas-challenge BOLD MR imaging methods to clinical settings, respiratory synchronization strategies such as bellows triggering (39), diaphragm navigating (40), and respiratory self-gating (41) may be critical for avoiding image artifacts during these free-breathing examinations. Alternatively, breath holding could be used to avoid such respiratory motion artifacts. However, breath-holding requirements could limit the spatial resolution and/or the imaging coverage, and, thus, future studies would be necessary to determine the physiologic effect of breath holding on hepatic gas-challenge BOLD response.

In conclusion, carbogen gas-challenge BOLD MR imaging is a promising method for the noninvasive diagnosis and staging of diseases that alter the hemodynamic processes of the liver. In a rat model of DEN-induced fibrosis, we observed a significant inverse correlation between gas-challenge BOLD response and degree of liver fibrosis. Future studies to evaluate the effectiveness of these techniques in patients with liver fibrosis are warranted.

References

1. Friedman SL. Liver fibrosis: from bench to bedside. J Hepatol 2003;38(suppl 1):S38–S53.
2. Poynard T, Yuen MF, Ratziu V, Lai CL. Viral hepatitis C. Lancet 2003;362(9401):2095–2100.
3. Thampanitchawong P, Piratvisuth T. Liver biopsy: complications and risk factors. World J Gastroenterol 1999;5(4):301–304.
4. Colloredo G, Guido M, Sonzogni A, Leandro G. Impact of liver biopsy size on histological evaluation of chronic viral hepatitis: the smaller the sample, the milder the disease. J Hepatol 2003;39(2):239–244.
5. Bedossa P, Dargere D, Paradis V. Sampling variability of liver fibrosis in chronic hepatitis C. Hepatology 2003;38(6):1449–1457.
6. Regev A, Berho M, Jeffers LJ, et al. Sampling error and intraobserver variation in liver biopsy in patients with chronic HCV infection. Am J Gastroenterol 2002;97(10):2614–2618.
7. Abdi W, Millan JC, Mezey E. Sampling variability on percutaneous liver biopsy. Arch Intern Med 1979;139(6):667–669.
8. Shiratori Y, Imazeki F, Moriyama M, et al. Histologic improvement of fibrosis in patients with hepatitis C who have sustained response to interferon therapy. Ann Intern Med 2000;132(7):517–524.
9. Poynard T, McHutchison J, Davis GL, et al. Impact of interferon alfa-2b and ribavirin on progression of liver fibrosis in patients with chronic hepatitis C. Hepatology 2000;32(5):1131–1137.
10. Nelson DR, Lauwers GY, Lau JY, Davis GL. Interleukin 10 treatment reduces fibrosis in patients with chronic hepatitis C: a pilot trial of interferon nonresponders. Gastroenterology 2000;118(4):655–660.
11. Huwart L, Peeters F, Sinkus R, et al. Liver fibrosis: non-invasive assessment with MR elastography. NMR Biomed 2006;19(2):173–179.
12. Koinuma M, Ohashi I, Hanafusa K, Shibuya H. Apparent diffusion coefficient measurements with diffusion-weighted magnetic resonance imaging for evaluation of hepatic fibrosis. J Magn Reson Imaging 2005;22(1):80–85.
13. Aube C, Oberti F, Korali N, et al. Ultrasonographic diagnosis of hepatic fibrosis or cirrhosis. J Hepatol 1999;30(3):472–478.
14. Talwalkar JA, Kurtz DM, Schoenleber SJ, West CP, Montori VM. Ultrasound-based transient elastography for the detection of hepatic fibrosis: systematic review and meta-analysis. Clin Gastroenterol Hepatol 2007;5(10):1214–1220.
15. Pandharipande PV, Krinsky GA, Rusinek H, Lee VS. Perfusion imaging of the liver: current challenges and future goals. Radiology 2005;234(3):661–673.
16. Hittmair K, Gomiscek G, Langenberger K, Recht M, Imhof H, Kramer J. Method for the quantitative assessment of contrast agent uptake in dynamic contrast-enhanced MRI. Magn Reson Med 1994;31(5):567–571.
17. Chiandussi L, Greco F, Sardi G, Vaccarino A, Ferraris CM, Curti B. Estimation of hepatic arterial and portal venous blood flow by direct catheterization of the vena porta through the umbilical cord in man: preliminary results. Acta Hepatosplenol 1968;15(3):166–171.
18. Richter S, Mucke I, Menger MD, Vollmar B. Impact of intrinsic blood flow regulation in cirrhosis: maintenance of hepatic arterial buffer response. Am J Physiol Gastrointest Liver Physiol 2000;279(2):G454–G462.
19. Gulberg V, Haag K, Rossle M, Gerbes AL. Hepatic arterial buffer response in patients with advanced cirrhosis. Hepatology 2002;35(3):630–634.
20. Materne R, Smith AM, Peeters F, et al. Assessment of hepatic perfusion parameters with dynamic MRI. Magn Reson Med 2002;47(1):135–142.
21. Van Beers BE, Materne R, Annet L, et al. Capillarization of the sinusoids in liver fibrosis: noninvasive assessment with contrast-enhanced MRI in the rabbit. Magn Reson Med 2003;49(4):692–699.
22. Yoo HJ, Lee JM, Lee MW, et al. Hepatocellular carcinoma in cirrhotic liver: double-contrast-enhanced, high-resolution 3.0T-MR imaging with pathologic correlation. Invest Radiol 2008;43(7):538–546.
23. Annet L, Materne R, Danse E, Jamart J, Horsmans Y, Van Beers BE. Hepatic flow parameters measured with MR imaging and Doppler US: correlations with degree of cirrhosis and portal hypertension. Radiology 2003;229(2):409–414.
24. Cao Y, Welch KM, Aurora S, Vikingstad EM. Functional MRI-BOLD of visually triggered headache in patients with migraine. Arch Neurol 1999;56(5):548–554.
25. Toni I, Krams M, Turner R, Passingham RE. The time course of changes during motor sequence learning: a whole-brain fMRI study. Neuroimage 1998;8(1):50–61.
26. Taylor NJ, Baddeley H, Goodchild KA, et al. BOLD MRI of human tumor oxygenation during carbogen breathing. J Magn Reson Imaging 2001;14(2):156–163.
27. Egred M, Al-Mohammad A, Waiter GD, et al. Detection of scarred and viable myocardium using a new magnetic resonance imaging technique: blood oxygen level dependent (BOLD) MRI. Heart 2003;89(7):738–744.
28. Meyer RA, Towse TF, Reid RW, Jayaraman RC, Wiseman RW, McCully KK. BOLD MRI mapping of transient hyperemia in skeletal muscle after single contractions. NMR Biomed 2004;17(6):392–398.
29. Ries M, Basseau F, Tyndal B, et al. Renal diffusion and BOLD MRI in experimental diabetic nephropathy: blood oxygen level-dependent. J Magn Reson Imaging 2003;17(1):104–113.

30. Barash H, Gross E, Matot I, et al. Functional MR imaging during hypercapnia and hyperoxia: noninvasive tool for monitoring changes in liver perfusion and hemodynamics in a rat model. Radiology 2007;243(3):727–735.

31. Barash H, Gross E, Edrei Y, et al. Functional magnetic resonance imaging monitoring of pathological changes in rodent livers during hyperoxia and hypercapnia. Hepatology 2008;48(4):1232–1241.

32. Galbraith SM, Lodge MA, Taylor NJ, et al. Reproducibility of dynamic contrast-enhanced MRI in human muscle and tumours: comparison of quantitative and semi-quantitative analysis. NMR Biomed 2002;15(2):132–142.

33. Blendis L, Wong F. The hyperdynamic circulation in cirrhosis: an overview. Pharmacol Ther 2001;89(3):221–231.

34. Zoli M, Magalotti D, Bianchi G, et al. Functional hepatic flow and Doppler-assessed total hepatic flow in control subjects and in patients with cirrhosis. J Hepatol 1995;23(2):129–134.

35. Newell P, Villanueva A, Friedman SL, Koike K, Llovet JM. Experimental models of hepatocellular carcinoma. J Hepatol 2008;48(5):858–879.

36. Duyn JH, Moonen CT, van Yperen GH, de Boer RW, Luyten PR. Inflow versus deoxyhemoglobin effects in BOLD functional MRI using gradient echoes at 1.5 T. NMR Biomed 1994;7(1-2):83–88.

37. Powell ME, Collingridge DR, Saunders MI, Hoskin PJ, Hill SA, Chaplin DJ. Improvement in human tumour oxygenation with carbogen of varying carbon dioxide concentrations. Radiother Oncol 1999;50(2):167–171.

38. Baron R, Baron Y, Disbrow E, Roberts TP. Brain processing of capsaicin-induced secondary hyperalgesia: a functional MRI study. Neurology 1999;53(3):548–557.

39. Low RN, Alzate GD, Shimakawa A. Motion suppression in MR imaging of the liver: comparison of respiratory-triggered and nontriggered fast spin-echo sequences. AJR Am J Roentgenol 1997;168(1):225–231.

40. Wang Y, Rossman PJ, Grimm RC, Riederer SJ, Ehman RL. Navigator-echo–based real-time respiratory gating and triggering for reduction of respiration effects in three-dimensional coronary MR angiography. Radiology 1996;198(1):55–60.

41. Larson AC, Kellman P, Arai A, et al. Preliminary investigation of respiratory self-gating for free-breathing segmented cine MRI. Magn Reson Med 2005;53(1):159–168.